Journal of Marine Science and Technology, Vol. 28, No. 4, pp. 288-297 (2020)
DOI: 10.6119/JMST.202008_28(4).0007

SHIP ROUTING DETERMINATION BY VIRTUAL MEASUREMENTS OF AN INTEGRATED SYSTEM

Tsai-Hsin Chang[1] and Jian-Qun Hou [2]

Key words: ship-integrated system, GPS, INS, virtual measurement.

ABSTRACT

According to the requirements of international maritime organization model course 7.03, electronic navigation systems are essential for project pilots. Global positioning system (GPS) is currently the most widely used electronic navigation equipment. However, because of the frequent blockages of GPS signals in complex environments, obtaining a precise and real-time position is difficult. To satisfy the requirement of effective and stable positioning of ship berthing and unberthing, another independent navigation system, inertial navigation system (INS), was adopted. In this study, we developed a 2-dimension (2D) GPS/INS-integrated system by using the constraint of a ship moving on a plane. If GPS signals are unavailable, virtual measurement is adopted to obtain some information on the ship position by considering ship constraints. A loose coupled approach using the extended Kalman filter (EKF) was proposed to obtain integrated solutions. The simulation and dynamic experimental results indicated that the 2D integrated system is adequate for ship navigation, and that the proposed methodology substantially enhances the performance of navigation systems.

I. INTRODUCTION

Traditional ship navigation methods, such as landmark positioning, are applicable only to locally known targets and are subject to environmental and line-of-sight restrictions. Dead reckoning requires measurement of the direction, speed, and time, which can easily cause an error (Diamant and Jin, 2014). Celestial positioning computation is complex and affected by weather conditions at twilight (Han and Li, 2016).

From its introduction in the 1970s, GPS has been widely used in civil navigation systems. In May 2000, the U.S. government discontinued selective availability, thereby substantially improving the GPS positioning accuracy. SOLAS regulation V/19.2.1.6 requires all ships, irrespective of their size, to have a receiver for a global navigation satellite, terrestrial radio navigation, or other system, suitable to be used at all times throughout the intended voyage to determine and update the ship position through automatic systems. GPS presents excellent performance for ship navigation and has become the majorly used equipment for ship electronic navigation.

GPS exhibits excellent positioning performance in the case of satellite health and good dilution of precision (DOP) (Farrell and Barth, 1999; Misra and Enge, 2001). However, its dynamic property and antijamming capacity are poor. By contrast, inertial navigation systems (INSs) can independently navigate and offer a message on the attitude, velocity, and position of vehicles without external signals (Huang et al., 2017). INS exhibits a higher antijamming capacity than GPS does; however, it is associated with the problem of positioning error accumulation (Hyun et al., 2009). A GPS/INS-integrated system can eliminate the limitations of both systems and enhance the overall system. Therefore, the GPS/INS-integrated system has been recognized for providing continuous positioning services (Li et al., 2014; Moreo et al., 2007; Kim et al., 2010; Xu et al., 2018).

To solve the problem of positioning a single system, a 2D GPS/INS integration method was established, in which a loosely coupled model was formulated, and an extended Kalman filter (EKF) (Brown and Hwang. , 2012; Ding et al., 2007; Simon, 2006) was then applied to estimate the ship position. Even when no satellite is in view, we could obtain some positioning solution through virtual measurements (Xin et al., 2003). Assume that the ship is moving on a plane, and that its speed is not varying considerably. The information on the ship speed, which may be obtained by measurement using a Doppler speed log, is essential for favorable virtual measurements. Algorithm performance was verified using simulations and dynamic experimental results. The proposed methodology yielded a successful algorithm to overcome the ill-conditioned GPS positioning problem. The continuous positioning services of the ship based on the proposed methodology can be improved substantially.

The rest of this paper is organized as follows. Section II presents the concept of plane rotation and a brief review of GPS and INS measurements. Section III presents 2D mathematical modeling for the ship position and attitude dynamic equation. Section IV describes an approach to implementation

Paper submitted 12/07/18; revised 12/26/19; accepted 07/30/20. Corresponding Author: Tsai-Hsin Chang (Email: thchang618@mail.tumt.edu.tw)
[1] Department of Navigation, Taipei University of Marine Technology, Taipei,Taiwan, R.O.C.
[2] Kinpo Electronics, Inc

of GPS/INS integration. Several detailed case designs that analyze processing of the GPS/INS position are provided and applied to dynamic environments. Section V presents the simulation and experimental results. Virtual measurement is effective and efficient. Equipped with this scheme, the service of a GPS receiver can be sustained for a few minutes even when no satellite is available in the view. Section VI presents the conclusions

II. SENSOR OBSERVATION

1. GPS measurement

GPS is based on the time-of-arrival ranging method (Kaplan and Hegarty, 2017). The GPS receiver contains an internal clock used to determine the time required for signal propagation from the satellite to receiver. The receiver and satellite clock errors bias the range measurements; therefore, these measurements are referred to as pseudoranges.

Let p^i be the pseudorange from the receiver located at $\mathbf{r}=(x,y,z)$ in a WGS-84 coordinate system to the *i*-th satellite at $\mathbf{r}^i=(x^i,y^i,z^i)$. After an ionospheric delay, a tropospheric delay, and satellite clock errors are properly compensated, the pseudorange with respect to the *i*-th satellite can be modeled as follows:

$$p^i=\sqrt{(x-x^i)^2+(y-y^i)^2+(z-z^i)^2}+b+\varepsilon^i, \qquad (1)$$

where $b=cdt$ is the product of the clock error of the receiver dt and speed of light c, and ε^i represents an unmodeled error. A total of four unknowns are observed, and measurements from at least four satellites in the field of view are required. In particular, assume that >4 satellites are in the view; thus, the least square method can be applied to determine the position and clock bias of the receiver. If the number of visible satellites decreases below four, the number of equations becomes insufficient for a unique solution. The proposed virtual measurement and integrated system can overcome such ill-conditioned problems. To evaluate the capacity of virtual measurements, several tests are performed (Section V).

2. INS measurement

INS is a self-contained and continuous navigation system that is independent of the detection of external signals; thus, it is immune to jamming and deception. INS measurements obtained from accelerometers and gyroscopes (gyros) are used to track the position and orientation of an object relative to a known starting point, orientation, and velocity. Unbounded growth in the position and velocity errors caused by integration of inertial measurements results in various errors that can adversely affect measurements. Many specific INS implementation approaches based on design decisions regarding coordinate systems, sensor suite, and rotation matrix computations are achievable. We use a strap-down system for inertial navigation applications. A strap-down platform is rigidly attached to the vehicle (ship). Its coordinate axes are usually nominally defined to have the same directions as the vehicle axes.

The basic idea of pure INS is to integrate acceleration signals to determine the velocity and position on a desired coordinate system. Assume an accelerometer as a spring mass damper system, in which the specific force $\mathbf{f}$ can be measured as follows:

$$\mathbf{f}=\ddot{\mathbf{r}}-\mathbf{G(r)}, \qquad (2)$$

where $\mathbf{r}$ represents the inertial position vector, and $\mathbf{G(r)}$ denotes the position-dependent gravitational acceleration. Consider that accelerometer casing is the gravitational field of the earth and is rotating about the earth at earth rotation rate. From Eq. (2), the accelerometer output equation is as follows:

$$\mathbf{f}=\mathbf{\Omega}_{ie}\mathbf{\Omega}_{ie}\mathbf{r}-\mathbf{G(r)}, \qquad (3)$$

where

$$\mathbf{\Omega}_{ie}=\begin{bmatrix}0 & -(\omega_{ie})_3 & (\omega_{ie})_2\\ (\omega_{ie})_3 & 0 & -(\omega_{ie})_1\\ -(\omega_{ie})_2 & (\omega_{ie})_1 & 0\end{bmatrix}=[\omega_{ie}\times], \qquad (4)$$

where ω_{ie} is the inertial angular rate vector of the earth, assuming that the inertial-frame origin is coincident with the center of the earth. Index $(\ )_i$, i = 1, 2, 3 denotes three components of ω_{ie}.

In the case of plane motion, we can use two accelerometers and one gyroscope for navigation. In the strap-down system, angular rates are measured at platform coordinates and are integrated to obtain the overall change in attitude over time. The major error sources of accelerometers and gyro only include bias and white noise. The measurements are such that

$$\begin{cases}\tilde{\mathbf{f}}=\mathbf{f}+b_a+\xi_a\ ; & \dot{b}_a=\eta_a\ , \qquad (5a)\\ \tilde{\omega}_{ip}^p=\omega_{ip}^p+b_g+\xi_g\ ; & \dot{b}_g=\eta_g\ , \qquad (5b)\end{cases}$$

where $\mathbf{f}$ denotes the true specific force; ω_{ip}^p is the true inertial angular rate of the platform frame expressed in platform coordinates; indices *a* and *g* denote the accelerometer and gyro, respectively; *b* is the bias; and ξ and η are white noise described by normal distributions.

III. 2D KINEMATIC MODELING OF SHIP

1. Positioning dynamic equations

For navigation, the local geodetic frame used is a north, east, down (NED) rectangular coordinate system. It is determined

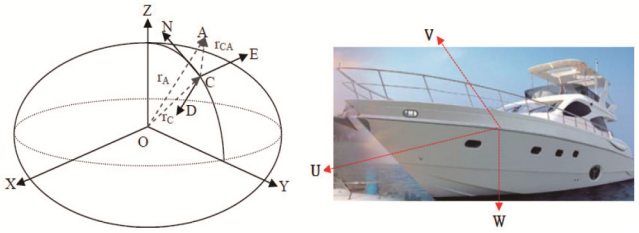

(a) (b)

Fig. 1. Reference coordinates system of (a) local frame (N, E, D) and (b) body frame (U, V, W).

by fitting a tangent plane to a geodetic reference ellipse at an interest point C, cf. Fig. 1.

This local coordinate system is attached to a fixed point on the surface of the earth, that is, it rotates with the rotation of the earth. The position vector $\mathbf{r}_{CA}$ is directed from the local frame origin C to the vehicle A (Fig. 1). The usual rectangular coordinate systems (X, Y, Z) are referred to as the earth-centered inertial (ECI) coordinate system. If the angular acceleration of the earth rotation is zero, then

$$\begin{cases} \dot{\mathbf{r}}_{CA}\big|_i = \dot{\mathbf{r}}_{CA}\big|_l + \omega_e \times \mathbf{r}_{CA} , & (6a) \\ \ddot{\mathbf{r}}_{CA}\big|_l = \ddot{\mathbf{r}}_{CA}\big|_i - 2\times\omega_e \times \dot{\mathbf{r}}_{CA}\big|_l - \omega_e \times (\omega_e \times \mathbf{r}_{CA}) , & (6b) \end{cases}$$

where $\dot{\mathbf{r}}_{CA}\big|_i$ and $\dot{\mathbf{r}}_{CA}\big|_l$ denote the time derivative of the vector $\mathbf{r}_{CA}$ relative to ECI and local frames, respectively; ω_e is the angular velocity vector of the earth rotation; $2\times\omega_e\times\dot{\mathbf{r}}_{CA}\big|_l$ is the Coriolis acceleration; and $\omega_e\times(\omega_e\times\mathbf{r}_{CA})$ is the acceleration caused by the earth rotation. Under this assumption, we have

$$\begin{cases} \dot{\mathbf{r}}_{C}\big|_i = \omega_e \times \mathbf{r}_C , & (7a) \\ \ddot{\mathbf{r}}_{C}\big|_i = \omega_e \times (\omega_e \times \mathbf{r}_C) . & (7b) \end{cases}$$

From Eqs. (2) and (7b), $\ddot{\mathbf{r}}_{CA}\big|_i$ can be derived as follows:

$$\ddot{\mathbf{r}}_{CA}\big|_i = \ddot{\mathbf{r}}_{A}\big|_i - \ddot{\mathbf{r}}_{C}\big|_i = \mathbf{f} + \mathbf{G}(\mathbf{r}_A) - \omega_e \times (\omega_e \times \mathbf{r}_C) . \quad (8)$$

Substituting Eq. (8) into (6a), $\ddot{\mathbf{r}}_{CA}\big|_l$ can be established as follows

$$\begin{aligned} \ddot{\mathbf{r}}_{CA}\big|_l &= \mathbf{f} + \mathbf{G}(\mathbf{r}_A) - \omega_e \times (\omega_e \times \mathbf{r}_C) \\ &\quad - 2\times\omega_e \times \dot{\mathbf{r}}_{CA}\big|_l - \omega_e \times (\omega_e \times \mathbf{r}_{CA}) \\ &= \mathbf{f} - 2\times\omega_e \times \dot{\mathbf{r}}_{CA}\big|_l + g \end{aligned} , \quad (9)$$

where $g \equiv \mathbf{G}(\mathbf{r}_A) - \omega_e \times \omega_e \times \mathbf{r}_A$ is the local gravity vector. For the case when g only acts in the D direction of the NED frame, the independent dynamic equations could be written as follows:

$$\begin{cases} \dot{P}_N = V_N \\ \dot{P}_E = V_E \\ \dot{P}_D = V_D \\ \dot{V}_N = f_N - 2V_E\omega_{ie}\sin\lambda_C \\ \dot{V}_E = f_E + 2V_N\omega_{ie}\sin\lambda_C + 2V_D\omega_{ie}\cos\lambda_C \\ \dot{V}_D = f_D - 2V_E\omega_{ie}\cos\lambda_C + g_D \end{cases} , \quad (10)$$

where $P_{(\,)}$ and $V_{(\,)}$ denote the vehicle position and velocity in (N, E, D) components, respectively; $\omega_{ie} = 7{,}292{,}115*10^{-11}\,rad/\sec$ is the angular velocity of the earth rotation.

2. Attitude

Consider the situation illustrated in Fig. 1. The relation between local and body coordinate systems can be completely described by the rotation matrix $\mathbf{R}_l^b$. This rotation matrix can be defined as a series of three plane rotations involving Euler angles (roll φ, pitch θ, and yaw ψ), we have, cf. [3],

$$\mathbf{R}_l^b = \begin{bmatrix} \cos\psi\cos\theta & \sin\psi\cos\theta & -\sin\theta \\ -\sin\psi\cos\varphi + \cos\psi\sin\theta\sin\varphi & \cos\psi\cos\varphi + \sin\psi\sin\theta\sin\varphi & \cos\theta\sin\varphi \\ \sin\psi\sin\varphi + \cos\psi\sin\theta\sin\varphi & -\cos\psi\sin\varphi + \sin\psi\sin\theta\cos\varphi & \cos\theta\cos\varphi \end{bmatrix} . \quad (11)$$

From Eq. (11), the specific force vector in the local frame $\mathbf{f}^l = [f_N, f_E, f_D]$ can be calculated based on the body frame $\mathbf{f}^b = [f_U, f_V, f_W]$ measurements.

$$\mathbf{f}^l = \begin{bmatrix} \cos\psi\cos\theta & -\sin\psi\cos\varphi + \cos\psi\sin\theta\sin\varphi & \sin\psi\sin\varphi + \cos\psi\sin\theta\sin\varphi \\ \sin\psi\cos\theta & \cos\psi\cos\varphi + \sin\psi\sin\theta\sin\varphi & -\cos\psi\sin\varphi + \sin\psi\sin\theta\cos\varphi \\ -\sin\theta & \cos\theta\sin\varphi & \cos\theta\cos\varphi \end{bmatrix} \mathbf{f}^b . \quad (12)$$

If angular rate gyros are rigidly mounted on the vehicle, the linear differential equation describing the dynamic can be expressed as follows:

$$\begin{bmatrix} \dot{\varphi} \\ \dot{\theta} \\ \dot{\psi} \end{bmatrix} = \begin{bmatrix} 1 & \sin\phi\tan\theta & \cos\phi\tan\theta \\ 0 & \cos\phi & -\sin\phi \\ 0 & \dfrac{\sin\phi}{\cos\theta} & \dfrac{\cos\phi}{\cos\theta} \end{bmatrix} \begin{bmatrix} (\omega_{lb}^b)_1 \\ (\omega_{lb}^b)_2 \\ (\omega_{lb}^b)_3 \end{bmatrix} , \quad (13)$$

$$\omega_{lb}^b = \omega_{ib}^b - \omega_{il}^b , \quad (14)$$

where ω_{ib}^{b} and ω_{il}^{b} are the gyro outputs and rotational angular rate of the earth expressed in body coordinates, respectively. Eq. (14) can be written as follows:

$$\begin{bmatrix}(\omega_{lb}^{b})_1\\(\omega_{lb}^{b})_2\\(\omega_{lb}^{b})_3\end{bmatrix}=\begin{bmatrix}\omega_U\\\omega_V\\\omega_W\end{bmatrix}-R_l^b\begin{bmatrix}\omega_{ie}\cos\lambda_C\\0\\-\omega_{ie}\sin\lambda_C\end{bmatrix} \tag{15}$$

From Eqs. (13) and (15), the attitude dynamic equation is obtained as follows:

$$\begin{bmatrix}\dot{\varphi}\\\dot{\theta}\\\dot{\psi}\end{bmatrix}=\begin{bmatrix}1 & \sin\phi\tan\theta & \cos\phi\tan\theta\\0 & \cos\phi & -\sin\phi\\0 & \dfrac{\sin\phi}{\cos\theta} & \dfrac{\cos\phi}{\cos\theta}\end{bmatrix}\cdot\left(\begin{bmatrix}\omega_U\\\omega_V\\\omega_W\end{bmatrix}-R_l^b\begin{bmatrix}\omega_{ie}\cos\lambda_C\\0\\-\omega_{ie}\sin\lambda_C\end{bmatrix}\right) \tag{16}$$

3. Kinematic modeling

When the ship motion is on a plane and the positioning problem is transformed to a 2D problem, kinematic equations are under the following constraint conditions:

$$V_D=\dot{V}_D=0\ , \tag{17}$$

$$\phi=\dot{\phi}=0\ , \tag{18}$$

and

$$\theta=\dot{\theta}=0\ . \tag{19}$$

Assume that the error sources of the accelerometer and gyro include only bias and white noise obtained from Eqs. (5a) and (5b). Substituting Eqs. (17)–(19) in Eqs. (10), (12), and (16), the 2D kinematic modeling of ship is established as follows:

$$\begin{cases}\dot{P}_N=V_N\\\dot{P}_E=V_E\\\dot{V}_N=f_U\cos\psi-f_V\sin\psi-2V_E\omega_{ie}\sin\lambda_C\\\dot{V}_E=f_U\sin\psi+f_V\cos\psi+2V_N\omega_{ie}\sin\lambda_C\\\dot{\psi}=\omega_W+\omega_{ie}\sin\lambda_C\\\dot{b}_{aU}=\eta_{aU}\\\dot{b}_{aV}=\eta_{aV}\\\dot{b}_{gW}=\eta_{gW}\end{cases}. \tag{20}$$

where

$$f_U=\tilde{f}_U-b_{aU}+\xi_{aU}\ , \tag{21}$$

$$f_V=\tilde{f}_V-b_{aV}+\xi_{aV}\ , \tag{22}$$

and

$$\omega_W=\tilde{\omega}_W-b_{gW}+\xi_{gW}\ . \tag{23}$$

IV. GPS/INS-INTEGRATED SYSTEM

1. Extended Kalman filter review

The EKF is considerably adept in solving a particular problem of navigation systems, that is, integration of an INS with navigation data from other sensors, such as GPS data. The GPS/INS-integrated navigation system employs a loose coupled approach that can be implemented as EKF. Consider a nonlinear dynamical system with state equation $\mathbf{x}(t)$ and measurements $\mathbf{y}(t)$, which is expressed as follows:

$$\begin{aligned}\dot{\mathbf{x}}(t)&=\mathbf{g}(\mathbf{x}(t),\mathbf{u}(t),t)+\mathbf{n}(t)\ ,\\\mathbf{y}(t)&=\mathbf{h}(\mathbf{x}(t),t)+\mu(t)\ ,\end{aligned} \tag{24}$$

where ***g*** and ***h*** are the known functions; ***u*** is the control input; and the process noise ***n*** and measurement noise μ are the independent zero-mean Gaussian random processes. Now, assume that the reference state $\bar{\mathbf{x}}$ satisfies the following nonlinear system

$$\dot{\bar{\mathbf{x}}}(t)=\mathbf{g}(\bar{\mathbf{x}}(t),\mathbf{u}(t),t)\ , \tag{25}$$

$$\bar{\mathbf{y}}(t)=\mathbf{h}(\bar{\mathbf{x}}(t),t)\ , \tag{26}$$

and $\bar{\mathbf{x}}(0)\approx\mathbf{x}(0)$. Let $\mathbf{x}(t)=\bar{\mathbf{x}}(t)+\Delta\mathbf{x}$. Up to the first order, we have

$$\Delta\dot{\mathbf{x}}(t)=\mathbf{G}(\bar{\mathbf{x}}(t),\mathbf{u}(t),t)\Delta\mathbf{x}(t)+\mathbf{n}(t)\ , \tag{27}$$

$$\mathbf{z}(t)=\mathbf{y}(t)-\bar{\mathbf{y}}(t)=\mathbf{H}(\bar{\mathbf{x}}(t),t)\Delta\mathbf{x}(t)+\mu(t)\ , \tag{28}$$

where

$$\mathbf{G}(\bar{\mathbf{x}}(t),\mathbf{u}(t),t)=\left.\frac{\partial\mathbf{g}}{\partial\mathbf{x}}\right|_{\mathbf{x}=\bar{\mathbf{x}}}\ , \tag{29}$$

$$\mathbf{H}(\bar{\mathbf{x}}(t),t)=\left.\frac{\partial\mathbf{h}}{\partial\mathbf{x}}\right|_{\mathbf{x}=\bar{\mathbf{x}}}\ . \tag{30}$$

The estimate state $\hat{\mathbf{x}}_k$ must be determined at time t_k, and this estimate is based on a previous estimate $\hat{\mathbf{x}}_k^-$ with an error covariance matrix $\mathbf{P}_k^-$ and the new measurement. The initial estimate of the process is $\hat{\mathbf{x}}_0^-=\bar{\mathbf{x}}_0$. For measurement update and time propagation, refer to (Brown and Hwang, 2012).

The unobservable problem prevents estimation of the bias value of INS, so that attitude estimation is required in the integrated navigation system.

Although the number of visible satellites decreases to one or zero, virtual measurements can be used to provide some useful information to prevent divergence of the positioning error as soon as INS is directly estimated. The GPS/INS-integrated navigation system is mainly used for ships, and the ship speed can be obtained using the Doppler speed log. The effects of the virtual measurement and velocity for the integrated system are discussed by considering different cases.

2. Case A.

Ship velocity measurements are **not** included in the GPS/INS system, and INS measurements are directly used for estimation without GPS signals.

For the position, velocity, and attitude, 2D modeling is employed to describe the dynamical behavior of the ship. Let

$$\mathbf{x}_A = \left[P_N, P_E, V_N, V_E, \psi, b_{aU}, b_{aV}, b_{gW}\right]^T .$$

By applying Eq. (20) to the above equation, the state equation becomes

$$\dot{\mathbf{x}}_A = \begin{bmatrix} V_N \\ V_E \\ (\tilde{f}_U - b_{aU})\cos\psi - (\tilde{f}_V - b_{aV})\sin\psi - 2V_E\omega_{ie}\sin\lambda_C \\ (\tilde{f}_U - b_{aU})\sin\psi + (\tilde{f}_V - b_{aV})\cos\psi + 2V_N\omega_{ie}\sin\lambda_C \\ (\tilde{\omega}_W - b_{gW}) + \omega_{ie}\sin\lambda_C \\ \hline \mathbf{0}_{3*1} \end{bmatrix} + \begin{bmatrix} 0 & 0 & & \\ 0 & 0 & & \\ \cos\psi & -\sin\psi & | & \mathbf{0}_{4*4} \\ \sin\psi & \cos\psi & & \\ - & - & - & - \\ \mathbf{0}_{4*2} & & | & \mathbf{I}_{4*4} \\ & & | & \end{bmatrix} \begin{bmatrix} \xi_{aU} \\ \xi_{aV} \\ \xi_{gW} \\ \eta_{aU} \\ \eta_{aV} \\ \eta_{gW} \end{bmatrix} . \quad (31)$$

Treating the position, velocity, and 2D attitude as measurements, the output equation becomes

$$\mathbf{y}_A = \begin{bmatrix} P_{N\_GPS} \\ P_{E\_GPS} \\ V_{N\_GPS} \\ V_{E\_GPS} \\ \psi_{2Dm} \end{bmatrix} = \left[\mathbf{I}_{5*5} \quad | \quad \mathbf{0}_{5*3}\right] \mathbf{x}_A + \mathbf{n}_A , \quad (32)$$

where the subscript (*_GPS*) denotes the measurement obtained from the GPS receiver.

3. Case B.

Ship velocity measurements are **not** included in the GPS/INS system, and the virtual measurements are used for estimation without GPS signals.

The virtual measurements applied are the virtual attitude, velocity, and position. The virtual attitude $\dot{\psi}_{vir}$ can be obtained directly by calculating the output of the corrected gyro as follows:

$$\dot{\psi}_{vir} = \tilde{\omega}_W - b_{gW} . \quad (33)$$

The use of ship constraints in the 2D model, that is, the ship not slipping for a short period, provides the following virtual velocity:

$$\begin{cases} V_{U\_vir} = \tilde{f}_U - b_{aU}, \ V_{V\_vir} = 0 \\ V_{N\_vir} = V_{U\_vir}\cos\psi_{vir} \\ V_{E\_vir} = V_{U\_vir}\sin\psi_{vir} \end{cases} . \quad (34)$$

From Eq. (34), the virtual position can be obtained by

$$\begin{cases} \dot{P}_{N\_vir} = V_{N\_vir} \\ \dot{P}_{E\_vir} = V_{E\_vir} \end{cases} . \quad (35)$$

In the environment of the ill-conditioned GPS, from Eqs. (33)–(35), the EKF output becomes

$$\mathbf{y}_B = \begin{bmatrix} P_{N\_vir} \\ P_{E\_vir} \\ V_{N\_vir} \\ V_{E\_vir} \\ \psi_{vir} \end{bmatrix} = \left[\mathbf{I}_{5*5} \quad | \quad \mathbf{0}_{5*3}\right] \mathbf{x}_A + \mathbf{n}_B \quad (36)$$

A moving ship subjected to this virtual measurement reduces error divergence compared with *Case A*.

4. Case C.

Ship velocity measurements are **included** in the GPS/INS system, and virtual measurements are used for estimation without GPS signals.

In general, speed V_{speed} of ships can be measured from the Doppler speed log. This measurement usually contains a scale factor error; thus, we should estimate a scale factor K_V for correction. In this case, the EKF is used to estimate the state:

$$\mathbf{x}_B = \left[P_N, P_E, V_N, V_E, \psi, b_{aU}, b_{aV}, b_{gW}, K_V\right]^T .$$

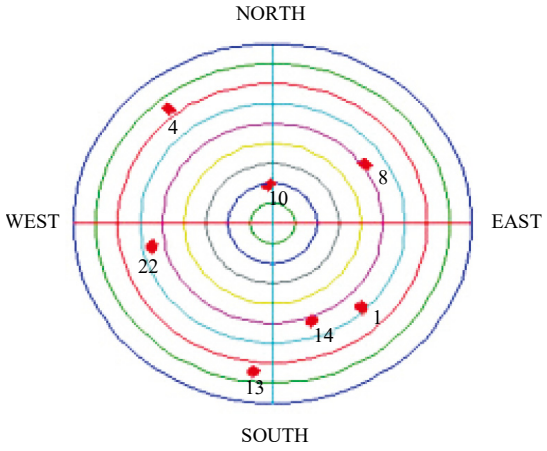

Fig. 2. Path of visible satellites in the sky.

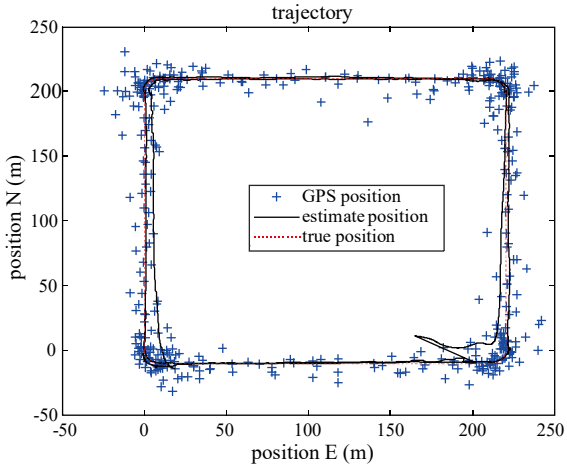

Fig. 3. Simulation results obtained using the normal GPS and integrated system.

If the ship is considered to exhibit no lateral sliding, the relationship is as follows:

$$\begin{cases} V_N = K_V V_{speed} \cos\psi \\ V_E = K_V V_{speed} \sin\psi \end{cases}. \tag{37}$$

From Eqs. (31) and (37), the state equation with speed measurement is as follows:

$$\dot{\mathbf{x}}_B = \begin{bmatrix} K_V V_{speed} \cos\psi \\ K_V V_{speed} \sin\psi \\ (\tilde{f}_U - b_{aU})\cos\psi - (\tilde{f}_V - b_{aV})\sin\psi - 2V_E\omega_{ie}\sin\lambda_C \\ (\tilde{f}_U - b_{aU})\sin\psi + (\tilde{f}_V - b_{aV})\cos\psi + 2V_N\omega_{ie}\sin\lambda_C \\ (\tilde{\omega}_W - b_{gW}) + \omega_{ie}\sin\lambda_C \\ \hline \mathbf{0}_{4*1} \end{bmatrix} + \begin{bmatrix} 0 & 0 & & \\ 0 & 0 & & \\ \cos\psi & -\sin\psi & | & \mathbf{0}_{4*4} \\ \sin\psi & \cos\psi & & \\ - & - & - & - \\ & \mathbf{0}_{5*2} & | & \mathbf{I}_{4*4} \\ & & | & \mathbf{0}_{1*4} \end{bmatrix} \begin{bmatrix} \xi_{aU} \\ \xi_{aV} \\ \xi_{gW} \\ \eta_{aU} \\ \eta_{aV} \\ \eta_{gW} \end{bmatrix}. \tag{38}$$

Including the information of the scale factor K_V in the state equation, we obtain another set of output equations:

$$\mathbf{y}_C = \begin{bmatrix} P_{N\_GPS} \\ P_{E\_GPS} \\ V_{N\_GPS} \\ V_{E\_GPS} \\ \psi_{2Dm} \end{bmatrix} = \begin{bmatrix} \mathbf{I}_{5*5} & | & \mathbf{0}_{5*4} \end{bmatrix} \mathbf{x}_B + \mathbf{n}_C . \tag{39}$$

When the number of useful satellites is not adequate and no satellite is in the view, the virtual attitude, velocity, and position are activated to obtain additional information. The modified output equation is

$$\mathbf{y}_D = \begin{bmatrix} P_{N\_vir} \\ P_{E\_vir} \\ V_{N\_vir} \\ V_{E\_vir} \\ \psi_{vir} \end{bmatrix} = \begin{bmatrix} \mathbf{I}_{5*5} & | & \mathbf{0}_{5*4} \end{bmatrix} \mathbf{x}_B + \mathbf{n}_D , \tag{40}$$

where

$$\begin{cases} V_{N\_vir} = K_V V_{speed} \cos\psi_{vir} \\ V_{E\_vir} = K_V V_{speed} \sin\psi_{vir} \end{cases}, \tag{41}$$

Subsequently, virtual measurements are incorporated into the EKF measurement equation to obtain a solution for the ill-conditioned GPS navigation problem. The simulation and experimental results revealed that the proposed methodology, *Case C*, led to an effective scheme.

V. SIMULATION AND EXPERIMENTAL RESULTS

1. Simulation scenario and results

Simulations were conducted to confirm whether the INS bias and scale factor K_V can be accurately estimated. We only compared ***case A*** and ***case C*** from the previous section. Computer codes were constructed using the Matlab 7.03 version software. To mimic GPS navigation, the commercial software Satellite Navigation (SATNAV) toolbox by GPSoft was employed to generate the satellite raw data. The toolbox allows determination of satellites available in the view when

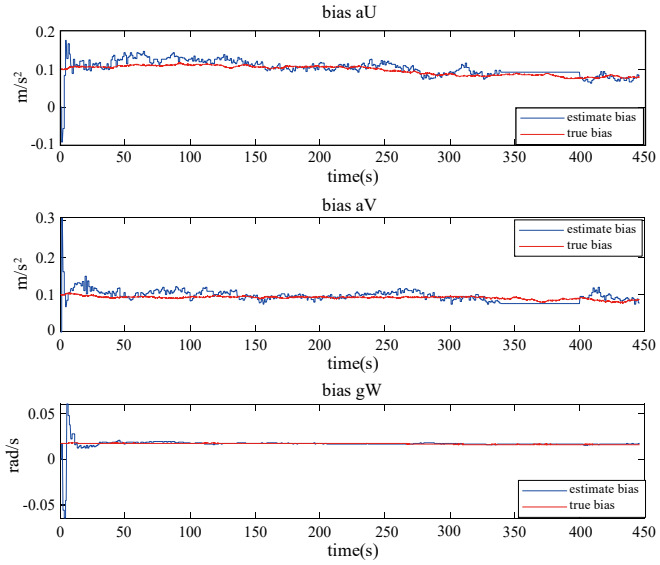

Fig.4. Estimated accelerometer bias and gyro bias using the *case A* scheme.

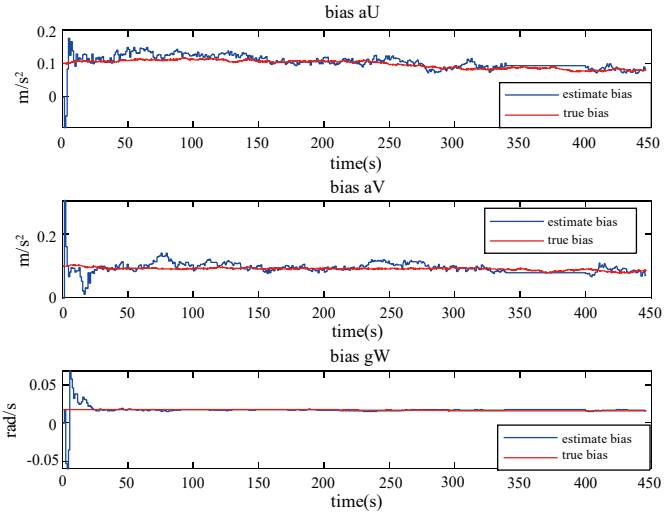

Fig. 5. Accelerometer and gyro bias estimated using the proposed scheme (*case C*).

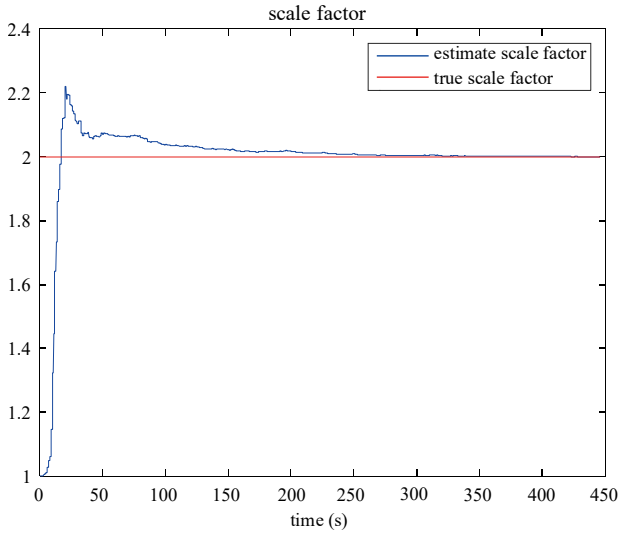

Fig. 6. Estimation of the scale factor K_V for *case C*.

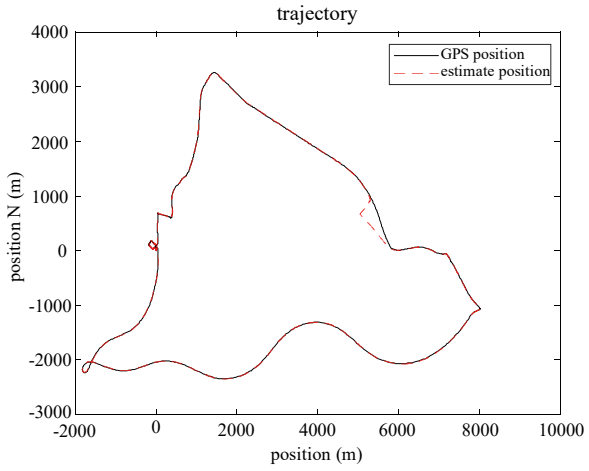

Fig. 7. 2-D positioning results obtained from the GPS receiver and integrated system by using *case A*.

the user position is specified. The satellite constellation was simulated, and error source corrupting GPS measurements included the ionospheric delay, tropospheric delay, thermal noise, and multipath error. Fig. 2 illustrates the visible satellites constellation emulation.

In this simulation, the standard deviation of the noise of ξ_a, η_a, ξ_g, and η_g is set to $0.3m/s^2$, $0.01m/s^2$, $1^\circ/s$ and $0.025^\circ/s$, respectively. Our designed trajectory is a square path. The simulation scenario is set with a vehicle trajectory moving from the position of [x-, y-, z-axis] = [−3025192.20, 4928782.54, 2681060.94] m in the WGS-84 ECEF coordinate system. The raw data are collected for 445 seconds, from 340 to 400 seconds, and the number of satellites is designed to be zero. Fig. 3 presents the 2D plot of trajectory and positioning results, such as the GPS normal position and position estimated using EKF.

In the ill-conditioned GPS environment, the INS bias (b_{aU}, b_{aV}, b_{gW}) was estimated through ***case A*** and ***case C*** approaches (Figs. 4 and 5). The information regarding the scale factor K_V should be included in the state equation for ***case C***, and Fig. 6 illustrates scale factor estimation. The simulations from ***case A*** and ***case C*** demonstrated that the bias and scale factor can be effectively estimated using the integrated navigation system for plane motion.

2. Dynamic Experiment

A dynamic experiment was conducted to assess the capacity of the proposed scheme (*case C*). In this experiment, an EverMore GPS receiver, analog device 2-axes accelerometers (ADXL203), and 1-axis gyro (ADXRS401) were selected because of their use in some navigators. The standard deviation

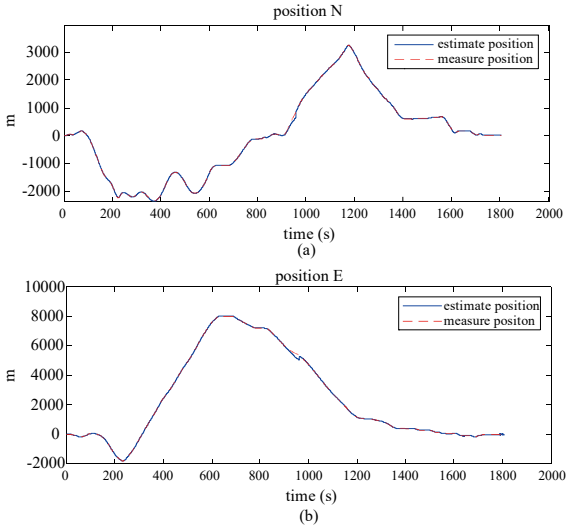

Fig. 8. Positioning results obtained from the GPS receiver by using the *case A* scheme. (a) North and (b) East directions.

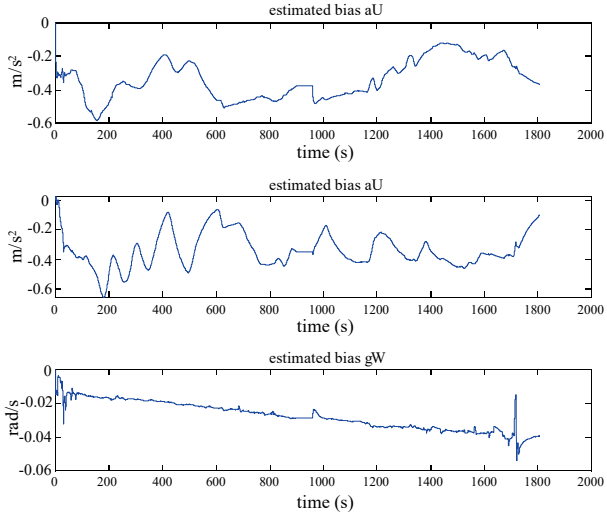

Fig. 10.Accelerometer and gyro bias estimated using the *case A* scheme in the dynamic experiment.

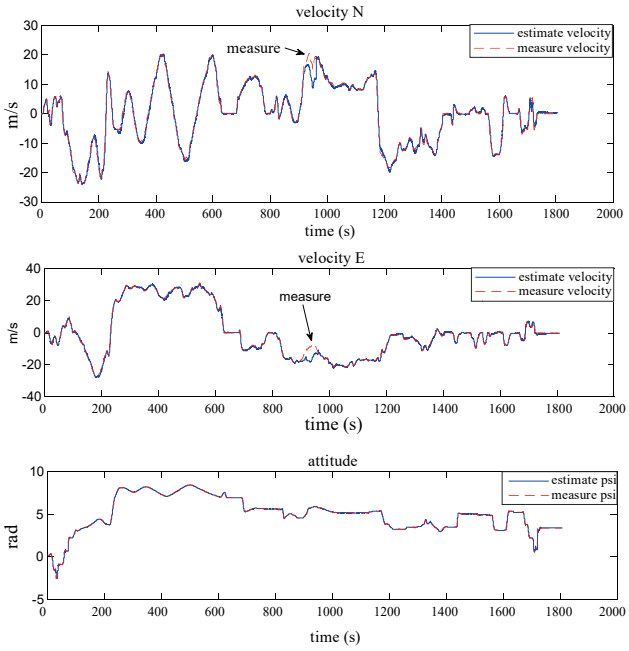

Fig. 9. Velocity and attitude results obtained from the GPS receiver by using the *case A* scheme.

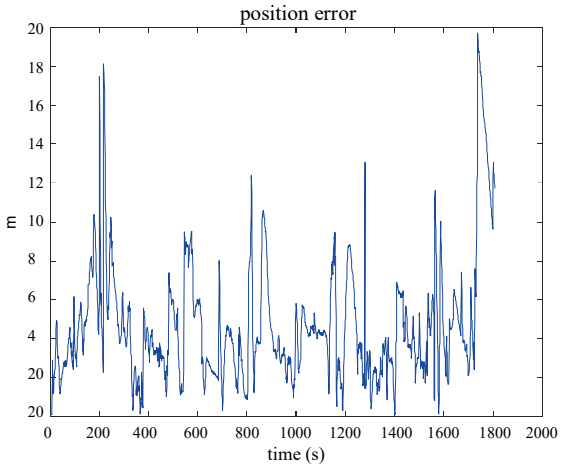

Fig. 11.Positioning error acquired using the *case A* scheme in the dynamic experiment (satellites are healthy).

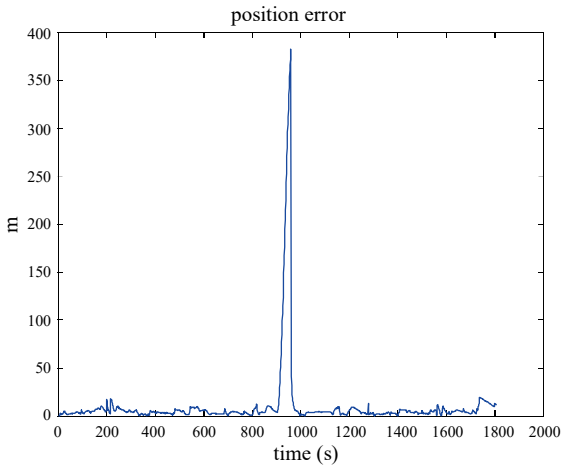

Fig. 12.Positioning error estimated using the *case A* scheme in the dynamic experiment (no visible satellites during 900~960 seconds).

of the noise ξ_a , η_a , ξ_g , and η_g of $0.07 m/s^2$, $0.001 m/s^2$, $0.6^\circ/s$, and $0.02^\circ/s$ were used in the 2D GPS/INS-integrated navigation system for dynamic experiments. Fig. 7 presents a plot of the normal positioning results obtained from the receiver and EKF estimation.

Fig. 8(a) and (b) presents the position in north and east directions, respectively. Fig. 9(a) and (b) presents a comparison between the east and north components of the velocity generated from measurement and estimation, respectively. Figs. 9(c) and 10 present the 2D attitude and INS bias, respectively.

Table 1. RMS and Var of position errors in the ill-conditioned environment.

Approach		Position error	
		RMS	Var
case A	E	34.55672181376630	1.16032239132243e+03
	N	16.78180814790490	2.80616711221141e+02
case B	E	12.71009068988854	1.54813630541760e+02
	N	15.71818291132365	2.34083162926554e+02
case C	E	7.57559654647544	57.36158390771051
	N	6.45808434693381	41.72904891272198

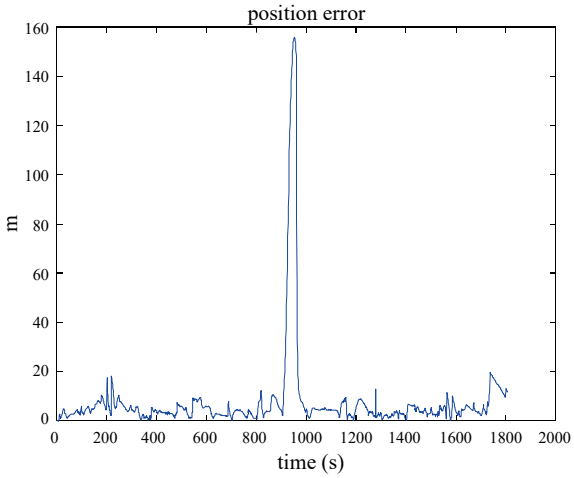

Fig. 13.Positioning error estimated using the *case B* scheme in the dynamic experiment (no visible satellites during 900~960 seconds).

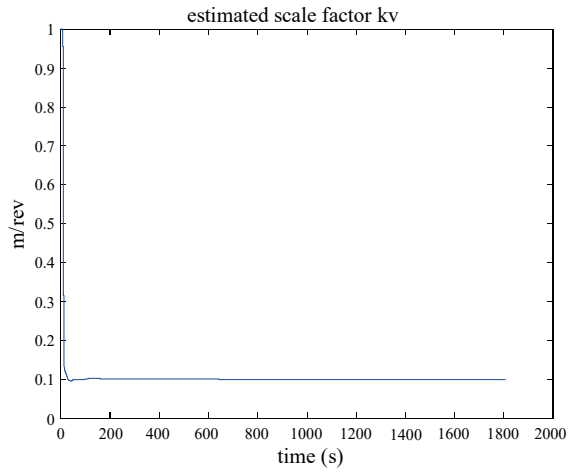

Fig. 14.Estimation of the scale factor K_V of *case C* in the dynamic experiment.

State variables were not divergent and can be estimated effectively. In the dynamic experiment, the estimated results were compared with GPS measurements to obtain the positioning error. The data was collected for 1808 seconds, and Fig. 11 illustrates the positioning error.

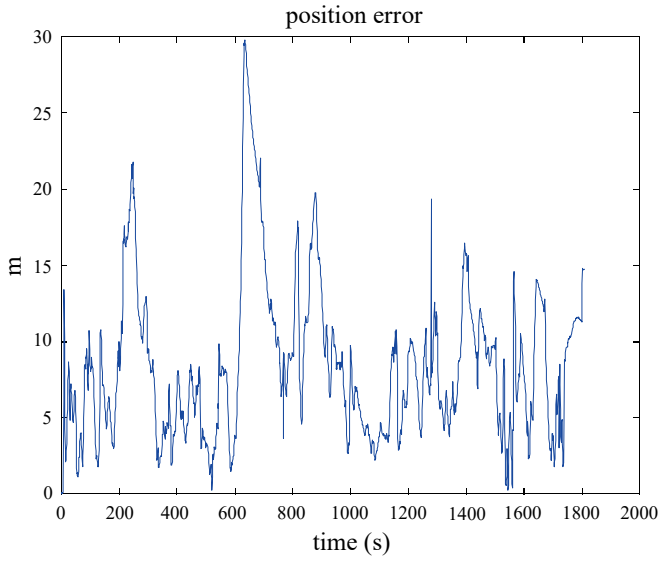

Fig. 15.Positioning error estimated using the proposed scheme (*case C*) in the dynamic experiment (satellites are healthy).

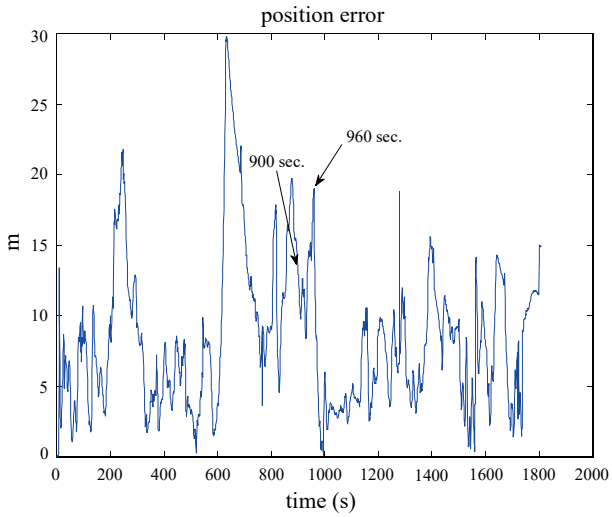

Fig. 16.Positioning error estimated using the proposed scheme (*case C*) in the dynamic experiment (no visible satellites during 900~960

From 900 to 960 seconds, the number of satellites was suddenly decreased to zero on purpose by deleting some pseudoranges. The methodology of *case A* and *case B* was then invoked with the positioning results presented in Figs. 12 and 13. The proposed virtual measurement could effectively reduce the positioning error.

Subsequently, the velocity and virtual measurement were used to obtain a complete solution for the ill-conditioned GPS positioning problem (*case C*). The change in the estimated INS bias to time in *case C* was similar to that in case A; thus, it did not present results. Fig. 14 presents the estimated scale factor K_V. Figs. 15 and 16 illustrate the positioning error of healthy satellite and GPS signal interruptions (900–960 seconds) and demonstrate that the proposed scheme (*case C*)

outperforms *case A* and *B*. When the number of satellites decreased to zero, the proposed method remained working, and Fig. 16 presents the results. Table 1 presents the root mean square (RMS) error and variances (Var) of using different cases. The results of dynamic experiment indicated that virtual measurements could substantially enhance the GPS positioning accuracy even in the ill-conditioned environment.

VI. CONCLUSIONS

Ships equipped with GPS may continue to satisfy SOLAS V/19.2.1.6 requirements; however, the problems of ill-conditioned GPS positioning frequently occur because of the environmental complexity. The special characteristics of motion were incorporated into the virtual measurement design to improve the positioning accuracy without GPS signals. In this study, the velocity and virtual measurements were used to provide a continuous service, even when the number of visible satellites was insufficient. The simulation and experimental results showed that if the ship motion satisfies the plane motion assumption, the INS bias can be effectively estimated. Although the 2D integrated navigation system using the virtual measurements can provide satisfactory positioning results, solving the navigation problem in the real environment with a 3D model to achieve the optimal navigation results remains necessary. Moreover, the covariance matrices of the process noise and measurement noise should be adjusted according to the complex environment. The proposed algorithm is being improved using the 3D model and adjusting covariance matrices, and the results will be reported later.

ACKNOWLEDGEMENT

The authors thank the Ministry of Science and Technology (MOST) (MOST 108-2635-E-229-001) for its helpful support.

REFERENCES

Brown ,R. G. and P. Y. C. Hwang (2012). Introduction to Random Signals and Applied Kalman Filtering with Matlab Exercises, 4th Edition. John Wiley & Sons.

Diamant, R. and Y.Jin (2014). A Machine Learning Approach for Dead-Reckoning Navigation at Sea Using a Single Accelerometer. IEEE Journal of Oceanic Engineering 39(4), 672-684.

Ding, W., J. Wang and C. Rizos (2007). Improving Adaptive Kalman Estimation in GPS/INS Integration. Journal of *Navigation* 60(3), 517–529.

Farrell ,J. A. and M. Barth (1999). The Global Positioning System and Inertial Navigation. McGraw-Hill.

Han, J., C.Wang and B. Li (2016). High accuracy method of positioning based on multi-star-sensor. Proceedings of Seventh International Conference on Intelligent Control and Information Processing (ICICIP), Siem Reap, Cambodia, 236–242.

Huang,H., X. Chen, Z.i Zhou, H. Liu and C. Lv (2017). Study on INS/DR integration navigation system using EKF/RK4 algorithm for inderwater gliders. Journal of Marine Science and Technology 25(1), 84–95.

Hyun, D. , H. S. Yang, G. H. Yuk and H. S. Park (2009). A dead reckoning sensor system and a tracking algorithm for mobile robots. Proceedings of IEEE Conference Mechatronics, Malaga, Spain, 1–6.

Kaplan ,E.D. and C.J. Hegarty (2017). Understanding GPS/GNSS: Principle and applications, 3th Edition Artech House, Boston.

Kim, J.H., J. Lyou and H.K. Kwak (2010). Vision coupled GPS/INS scheme for helicopter navigation. Journal of Marine Science and Technology 24(2), 4894–496.

Li, Z., J.Wang, B. Li and J. Gao (2014). GPS/INS/Odometer Integrated System Using Fuzzy Neural Network for Land Vehicle Navigation Applications. The Journal of Navigation 67(6), 967–983.

Misra, P. and P. Enge (2001). Global Positioning System: signals, measurements, and performance. Ganga-Jamuna Press.

Moreo, R.T., M. A. Zamora-Izquierdo, B. Úbeda-Miñarro and A. F. Gómez-Skarmeta (2007). High-Integrity IMM-EKF-based road vehicle navigation with low-cost GPS/SBAS/INS. Journal of IEEE Transactions on Intelligent Transportation Systems 8(3), 491-511.

Simon, D.(2006). Optimal State Estimation Kalman, H_∞ , and Nonlinear Approaches. John Wiley & Sons.

Xu, Q., X. Li and C.Y. Chan (2018). Enhancing Localization Accuracy of MEMS-INS/GPS/In-Vehicle Sensors Integration During GPS Outages. Journal of IEEE Transactions on Instrumentation and Measurement 99,1-13.

Xin M., S. Sukkarieh and J. Hyuk Kim(2003).Vehicle Model Aided Inertial Navigation. Proceedings of IEEE International Conference on Intelligent Transportation Systems, Shanghai, China, 1004-1009.